Our Reference: 200209306-1   PATENT

IN THE UNITED STATES PATENT AND TRADEMARK OFFICE

Applicants: Theodore I. Kamins et al.

Serial Number: 10/690,688

Filing Date: October 21, 2003

Confirmation No.:   6130

Examiner/Group Art Unit: Robert M. Kunemund/1722

Title: METHOD OF FORMING THREE-
                                   DIMENSIONAL NANOCRYSTAL
                                   ARRAY

DECLARATION PURSUANT TO 37 C.F.R. § 1.132

Commissioner for Patents
P.O. Box 1450
Alexandria, VA 22313-1450

Sir:

I, Theodore I. Kamins, hereby declare the following:

1.   I am one of the inventors of the above-identified application.

2.   I am a citizen of the United States, residing in Palo Alto,
California.

3.   I received a B.S. in Electrical Engineering from the University
of California, Berkeley, located in Berkeley, CA, in 1963.

4.   I received an M.S. in Electrical Engineering (Solid-State
Electronics) from the University of California, Berkeley, located in Berkeley, CA,
in 1965.

5.   I received a Ph.D. in Electrical Engineering (Solid-State
Electronics) from the University of California, Berkeley, located in Berkeley, CA,
in 1968.

S.N. 10/690,688 / Docket No.: 200209306-1 2

6. From 1968 to 1969, I was Acting Assistant Professor, Dept. of Electrical Engineering, University of California, Berkeley.

7. From 1969 to 1974, I worked at the Research and Development Laboratory of Fairchild Semiconductor, located in Palo Alto, CA.

8. In 1974, I joined Hewlett-Packard Laboratories ("HP Labs") in Palo Alto, California as a Member of the Technical Staff. I am currently a Principal Scientist in the Quantum Science Research group at HP Labs, where I am focusing on advanced nanostructured electronic materials and devices.

9. From 1999 to the present, I have been a Consulting Professor in the Electrical Engineering Department at Stanford University, located in Stanford, CA.

10. Throughout my career, I have investigated several topics, including materials and device-related areas (e.g., the development of UV-sensitive photodiodes); silicon-on-insulator and rapid thermal processing; advanced epitaxy and device technology for the silicon-germanium, heterojunction bipolar transistor; self-assembled nanostructures formed by lattice-mismatched epitaxial deposition and self-assembled nanowires grown by catalytically enhanced chemical vapor deposition.

11. After reviewing U.S. Patent No. 6,831,017, I submit that the '017 patent teaches the use of thermal and plasma chemical vapor deposition techniques (see Col. 5, lines 10-12) for nanowire growth.

12. The '017 patent states that "During plasma CVD growth, the inherent electric field produced by the plasma may help to vertically orient the nanowires 18 that are grown. An external electric field may also be applied to a plasma or thermal CVD growth chamber to enhance the uniformity (e.g., the verticality) of the nanowire alignment. A typical electric field strength that may be used to enhance nanowire alignment may be on the order of 700 V/cm." This statement indicates that the nanowires of Li must be thin enough to bend under the influence of the applied electric field, whether it is an external electric field or is provided by the plasma.

13. It is my understanding that an electric field strength of 700 V/cm is capable of aligning nanowires having diameters less than about 2 nm. (See paragraphs 15 et seq. below for a more detailed, related discussion.)

14. The '017 patent also teaches that an amorphous material (e.g., silicon oxide, polymers, spin-on-glass, see Col. 6, lines 21-49) may be used as a matrix surrounding the nanowires, contrary to the materials taught in our currently pending claims 7 and 30. I submit that a three-dimensional array of nanocrystals substantially totally surrounded by a second material is not achievable if an amorphous material is used as a matrix around crystalline nanowires. In the '017 patent, the nanowires are uniformly composed of a crystalline material, while the filling matrix material is amorphous and, therefore, different than the nanowire material.

15. I reviewed the paper by Gudiksen et al., entitled "Growth of nanowire supperlattice structures for nanoscale photonics and electronics", published in February 2002 in Nature Vol. 415, pages 617-620 (referred to herein as "the Nature Paper"). The Nature Paper teaches nanowires having about 20 nm diameters. The deflection of the nanowire in an electric field decreases as the inverse fourth power of the diameter. Field alignment works with a carbon nanotube having a diameter of about 1.4 nm. See, for example, A. Ural, et al., Applied Physics Letters, vol. 81, p. 3466 (28 October 2002) (a copy of which is attached hereto as Exhibit 1), where an electric field of ~1V/μm (10^4 V/cm) is cited as the electric field needed for alignment of CNTs. However, for a given material, when the diameter increases from 1.4 nm to 20 nm, the deflection decreases by a factor of 41,600. This decrease is partially offset to a factor of about 6000 by the higher value of Young's modulus for carbon nanotubes (about 6-7 times higher for CNT than for Si). Therefore, a field about 6000 times higher is needed for a Si nanowire with 20 nm diameter compared to a carbon nanotube with 1.4 nm diameter. Consequently, I submit that an impractically high value of conventionally applied electric field (~4×10^6 V/cm) is needed for significant deflection (alignment capability) of a 20 nm Si nanowire. For an electric field of

S.N. 10/690,688 / Docket No.: 200209306-1 4

700 V/cm, the achievable deflection for a 20 nm Si nanowire has a negligible value of <1 Å (0.1 nm).

16. I submit that it is not practical to apply such a large field using conventional techniques. On the contrary, one would need a very clever technique (which is outside of the skill set of the ordinarily skilled artisan) that would (1) supply the high field; (2) allow the precursor gas to reach the growing nanowire (quite difficult due to close spacing of the electrodes); (3) not geometrically impede growth; and (4) be compatible with a high temperature, gaseous ambient. The present Declarant is not aware of any technical references having taught or suggested achieving all four of the above requirements. For example, the Kam IEDM paper, *infra*, achieves (1), but not the other requirements.

17. Comparing the teachings of the '017 patent and the Nature Paper, I conclude that one skilled in the art would not be likely to combine such teachings. In fact, I submit that the ordinarily skilled artisan would be led away from combining the teachings of Li with the Nature Paper for the following reasons. Li teaches exposing relatively thin nanowires to an electric field to achieve vertical alignment. The nanowires of the Nature Paper have a relatively thick diameter. If one were to attempt to align the nanowires of the Nature Paper by applying an external electric field as taught by Li, such an electric field would have to be orders of magnitude higher than that taught in Li to vertically align the nanowires. Further, such a field cannot be applied by conventional means. This conclusion may be inferred from an analogous system, wherein an electric field of $\sim 10^7$ V/cm (~ 5 V applied across a 5 nm gap) is also needed to deflect the 25 nm-wide Si field plate of a nanoelectromechanical field-effect transistor (although the situation is slightly different: clamped at both ends, rather than cantilevered from one end). See, for example, H. Kam, et al., 2005 International Electron Devices Meeting, Washington DC, December 5-7, 2005, paper 19.2, a copy of which is attached hereto as Exhibit 2.

S.N. 10/690,688 / Docket No.: 200209306-1 5

18. If one ordinarily skilled in the art were to attempt alignment of the Nature Paper nanowires using the electric fields, plasma techniques and thermal techniques taught by Li, I believe he/she would either fail, or destroy at least one segment of the Nature Paper nanowires for the following reasons.

19. The electric fields used in Li's techniques would not be strong enough to align the Nature Paper nanowires with either an externally applied electric field or in a plasma. In a plasma, the net DC field, as mentioned above, is also only moderate (~KV/cm).

20. I submit that, without undue experimentation, the plasma taught in Li is likely to deleteriously affect at least one of the segments of the nanowires taught in the Nature Paper because, to my knowledge, plasma exposure should be carefully controlled to avoid damaging the materials which are exposed to the plasma. When two or more materials are exposed, the limits of allowable plasma parameters decreases so that it is difficult to provide enough energy to align the nanowire without damaging the more (chemically or mechanically) fragile of the materials in the segmented nanowire. Additionally, if the plasma is used to enable the growth reaction, it is difficult to grow the segment requiring higher energy without damaging the more fragile segment.

I hereby declare that all statements made herein of my own knowledge are true and that all statements made on information and belief are believed to be true; and further that these statements were made with the knowledge that willful false statements and the like so made are punishable by fine or imprisonment, or both, under § 1001 of Title 18 of the United States Code and, that such willful false statements may jeopardize the validity of the application or any patent issued thereon.

Theodore I. Kamins, PhD.   _August 25, 2006_
Theodore I. Kamins, Ph.D.   Date

Electric-field-aligned growth of single-walled carbon nanotubes on surfaces

Ant Ural, Yiming Li, and Hongjie Dai[a)]
Department of Chemistry and Laboratory for Advanced Materials, Stanford University, Stanford, California 94305

Aligned single-walled carbon nanotubes are grown onto the surfaces of SiO_2/Si substrates in electric fields established across patterned metal electrodes. Calculations of the electric field distribution under the designed electrode structures, the directing ability of electric fields, and the prevention of surface van der Waals interactions are used to rationalize the aligned growth. The capability of synthesizing oriented single-walled nanotubes on surfaces shall open up many opportunities in organized architectures of nanotubes for molecular electronics. © *2002 American Institute of Physics.* [DOI: 10.1063/1.1518773]

Obtaining organized single-walled carbon nanotube (SWNT) structures is a critical step towards interesting and practical devices of novel molecular wires.[1,2] With two approaches—post-growth assembly and *in situ* controlled growth—progress has been made to reach this goal. In both approaches, electric fields have been exploited to control the orientation of SWNTs,[3,4] utilizing the highly anisotropic polarizability of nanotubes.[5] *In situ* growth by chemical vapor deposition (CVD) in an electric field can direct the orientation of SWNTs, as shown by our group with the nanotubes in suspended form.[3]

While suspended SWNTs with directionality are important to mechanical and electromechanical studies and devices,[6] it is equally important to grow aligned nanotubes resting on surfaces. This ability will then allow successive patterned growth steps in electric fields to produce multiple sets of nanotubes aligned to various directions, and allow metallization and other integration steps to fabricate addressable devices, without the mechanical instability problems of suspended nanotubes. Here, we show that aligned SWNTs on surfaces can indeed be obtained by electric-field-directed CVD growth, with a rational choice of substrates, electrode materials, and structures. The mechanism for alignment involves suitable electric field distributions and the prevention of van der Waals binding with substrate surfaces during nanotube growth.

We started with Si wafers with 1.85-μm-thick thermally grown SiO_2 as substrates. We used molybdenum metal electrodes to establish electric fields on the substrates, as shown in Fig. 1(a). The electrodes were patterned by photolithography and liftoff, each with a dimension of 0.8 cm by 0.3 cm and a thickness of either 50 or 100 nm. The gap between the Mo electrodes was 10 μm. We then patterned a catalyst on top of the two opposing Mo electrodes using a second photolithography step aligned to the electrodes. The catalyst regions on the two electrodes were designed to be 5 μm × 0.4 cm strips containing an alumina supported Fe/Mo catalyst,[7] and were ~3–5 μm away from the edges of the Mo electrodes [Fig. 1(b)]. The catalyst patterning step uti-

lized a poly(methylmethacrylate) (PMMA) and photoresist double layer approach. The top photoresist layer was first patterned by standard photolithography. After developing, oxygen plasma was used to etch into and form wells in the PMMA. The top photoresist layer was then fully removed by exposure to a high flux of light and subsequent development. Catalyst material was then deposited from a methanol suspension into the patterned PMMA wells followed by liftoff in acetone.[7] We used the double layer approach so that PMMA can be patterned by standard photolithography and
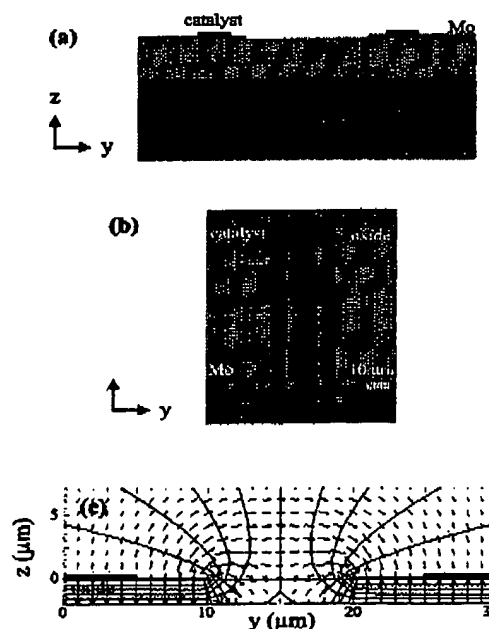

FIG. 1. Structure of samples used for electric field aligned growth of SWNTs on surfaces. (a) Cross-sectional view of the Si/SiO$_2$ (1.85-μm-thick) substrate, microfabricated Mo electrodes, and the catalyst strips (not to scale). The gap between the Mo electrodes is 10 μm. (b) An optical image showing the top-view of a sample. (c) Electric field distribution and equipotential lines calculated for the left and right Mo electrodes biased at 10 and 0 V, respectively. The underlying Si substrate is floating. The lengths of the field line arrows scale with the strengths of the local fields.

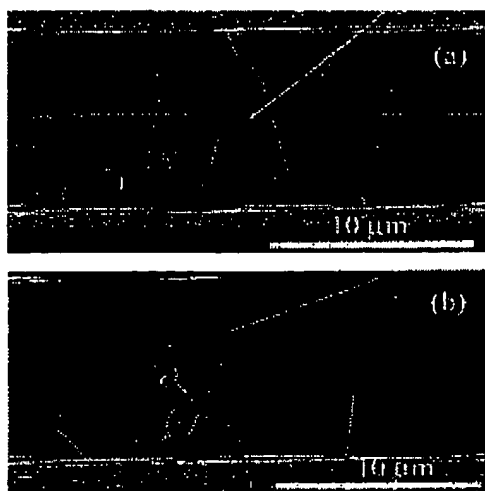[a)]Electronic mail: hdai1@stanford.edu

FIG. 2. Random orientations of nanotubes grown by CVD when no electric field is applied in a control experiment. The two AFM images show randomly oriented nanotubes in the gap region between the Mo electrodes. The edges of the Mo electrodes are shown at the top and bottom of each image.

dry etching. The photoresist pattern itself was not used for catalyst patterning due to the incompatibility of photoresist with methanol.

Aligned SWNTs across the gap between the electrodes were grown in a 1 in. CVD system equipped with electrical feedthroughs. The substrate was mounted on a home-made fixture on which two metal stainless steel clips were designed to make electrical contact to the Mo electrodes for applying bias voltages (3–20 V) across the gap. The Si substrate underlying the SiO₂ layer was kept floating. A 40 kΩ serial resistor was used to limit the current. SWNTs were

grown at 900 °C for 2 min under 720 mL/min of methane, 500 mL/min of hydrogen, and 12 mL/min of ethylene flow. Pure hydrogen was flown during heating and cooling the CVD system to prevent oxidation of the Mo electrodes by possible oxygen impurities.

The substrates used in the current work were SiO_2/Si wafers (instead of quartz used previously for aligned suspended SWNTs[3]). The 1.85-μm-thick thermally grown SiO_2 layer was found stable against electrical breakdown under 3–20 V applied across the Mo electrodes. Mo was used for electrodes in place of polysilicon, due to its compatibility with high temperature CVD growth conditions without loss of conductivity.[8] These substrate and electrode materials significantly facilitated the current work owing to their simplicity and ease of microfabrication.

Control experiments reveal that, in the absence of electric fields, nanotubes grown from the catalyst regions bridge the electrodes in random orientations, as shown in the atomic force microscopy (AFM) images in Fig. 2. In strong contrast, high degree of alignment is observed for nanotubes grown under applied electric fields between the Mo electrodes. Figure 3 shows AFM data recorded with samples grown by CVD with a 10 V bias voltage applied across the 10 μm gap between the electrodes. The nanotubes are clearly aligned perpendicular to the edges of the electrodes, in the direction of the electric field. Scanning electron microscopy (SEM) imaging has also revealed aligned nanotube structures along the electric field direction (Fig. 4). We have carried out nanotube growth under applied voltages of 3, 5, 10, and 20 V. Alignment appears to be less effective, although still present, when 3 V is applied across the 10 μm gap. On the other hand, no obvious improvement is observed in the alignment of nanotubes when the voltage is increased to 20 V. Further increase in voltage tends to break down the SiO₂ dielectric

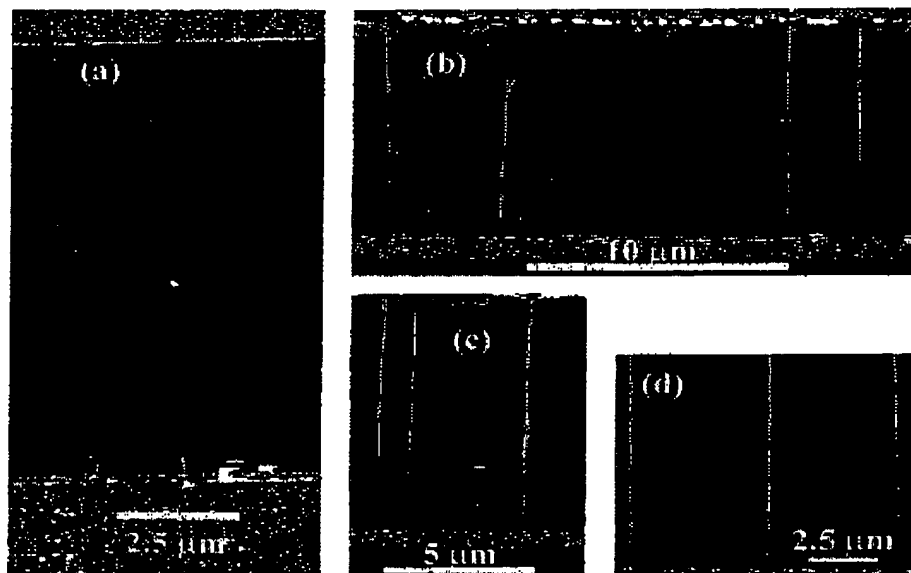FIG. 3. Aligned nanotubes resting on SiO₂ surfaces after electric field directed growth. The four images were obtained with different samples that had gone through independent electric-field-directed growth runs. The nanotubes show clear alignment in the direction of the electric field, perpendicular to the edges of the Mo electrodes.
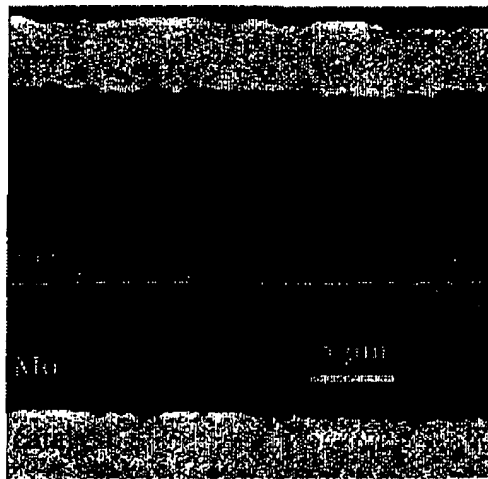
Ural, Li, and Dai

FIG. 4. An SEM image of aligned nanotubes grown by CVD in an electric field. The dark lines in the center region of the image are aligned nanotubes. The nanotubes and the Mo electrodes (regions bridged by the nanotubes) appear dark since they are electrically conducting, whereas the SiO_2 surface in the gap region appears bright due to charging effects under our imaging conditions. The catalyst strips are visible as the top and bottom bright areas.

layer. Thus, we identify that ~ 10 V applied between the electrodes spaced at 10 μm is optimum for aligned growth of nanotubes on surfaces. Using this condition, we have carried out growth with 20 samples, and observed a reproducible and consistent electric field alignment effect, with only slight variations in the degree of alignment from sample to sample.

To understand the alignment of nanotubes resting on SiO_2 surfaces, we first calculate the electric field distribution for our sample geometry using the MEDICI simulation program (by Avant! Co.) to solve the Laplace equation numerically. Fig. 1(c) shows a cross-section view of electric field vectors and equipotential lines for the sample structure. At the locations of the catalyst strips from which the nanotubes are grown, the electric field is nearly perpendicular to the Mo metal surface, with a field strength of ~ 0.5 V/μm. Right in the middle of the gap between the two metal electrodes, the electric field is 0.2 V/μm at the SiO_2–air interface. Note that the field lines in the gap are not perfectly parallel to the surface plane in the immediate vicinity of the surface, but are at a small angle. This is caused by the distortion effect of the floating Si substrate underneath the oxide layer.

We suggest that nanotubes grown from the catalyst regions initially extend into the air nearly normal to the metal electrode surface, along the direction of the local electric field. The nanotubes follow the electric field lines as they lengthen, and with the existence of field gradients, they tend to follow the field lines with the highest strength to maximize the interaction between the electric field and the induced dipole moments on the nanotubes.[3] When the nanotubes are over the electrode gap region, they are aligned to the overall field direction in the gap (perpendicular to the electrode edges on the $x–y$ plane), become directed towards the substrate by field gradients, and subsequently fall onto the surface. This results in aligned nanotubes immobilized on the surface by van der Waals forces.

There are two important factors for the aligned growth of SWNTs onto substrates. The first is the directing or aligning ability of the electric field. In our previous work, we have shown that in a field of ~ 1 V/μm, the induced dipole ($\sim 10^6$ Debye, largely along the tube axis due to the strong anisotropy in polarizability[5]) on a ~ 10 μm long SWNT is sufficient to overcome most of the orientation randomizing forces such as thermal vibration.[3] This condition is satisfied here since the electric field strength is on the order of 1 V/μm. An equally important factor is that during growth and lengthening, the nanotubes must stay away from surfaces to avoid capture by the surfaces, so that the nanotubes can fully experience the aligning effect of the electric field. For a nanotube pinned on a surface, strong van der Waals interactions will prevent it from responding to the field directing effect.[3] This condition is also satisfied by our sample design, as the nanotubes grown from the catalyst regions do not contact the substrate until they have been fully aligned to the electric field and guided onto the substrate.

A control experiment was carried out with the same substrate and electrode structures, but different catalyst locations. We placed catalyst, in the form of discrete Fe_2O_3 nanoparticles,[9] onto the SiO_2 surface in the gap region between the two Mo electrodes, and carried out CVD growth under a 10 V applied voltage across the 10 μm gap. The orientations of nanotubes thus grown appear random on the surface without any apparent alignment to the electric field direction inside the gap. We attribute this to the fact that the electric field direction is not normal to the surface at the catalyst sites in the gap region, and that field gradients in this region do not favor nanotubes directing away from the surface. Thus, once reaching a certain length at the early stage of growth, the nanotubes touch the substrate and become pinned.

In summary, we have used in situ electric fields to grow aligned SWNTs onto surfaces by CVD. Excellent alignment of nanotubes is obtained on SiO_2/Si surfaces based on a rational choice of materials and sample structure design. These results could lead to the synthesis of complex organized nanotube structures for molecular electronics applications.

[1] H. Dai, in Carbon Nanotubes, edited by M. S. Dresselhaus, G. Dresselhaus, and P. Avouris, eds. (Springer, Berlin, 2001), Vol. 80, p. 29.
[2] H. Dai, Surf. Sci. 500, 218 (2002).
[3] Y. Zhang, A. Chan, J. Cao, Q. Wang, W. Kim, Y. Li, N. Morris, E. Yenilmez, J. Kong, and H. Dai, Appl. Phys. Lett. 79, 3155 (2001).
[4] M. Diehl, S. Yaliraki, R. Beckman, M. Barahona, and J. Heath, Angew. Chem. Int. Ed. Engl. 41, 353 (2001).
[5] L. Benedict, S. G. Louie, and M. L. Cohen, Phys. Rev. B 52, 8541 (1995).
[6] T. Tombler, C. Zhou, L. Alexeyev, J. Kong, H. Dai, L. Liu, C. Jayanthi, M. Tang, and S. Y. Wu, Nature (London) 405, 769 (2000).
[7] J. Kong, H. Soh, A. Cassell, C. F. Quate, and H. Dai, Nature (London) 395, 878 (1998).
[8] N. R. Franklin, Q. Wang, T. W. Tombler, A. Javey, M. Shim, and H. Dai, Appl. Phys. Lett. 81, 913 (2002).
[9] Y. Li, W. Kim, Y. Zhang, M. Rolandi, D. Wang, and H. Dai, J. Phys. Chem. 105, 11424 (2001).

A New Nano-Electro-Mechanical Field Effect Transistor (NEMFET) Design for Low-Power Electronics

Hei Kam[1], Donovan T. Lee[1], Roger T. Howe[2], and Tsu-Jae King[1,3]

[1]Dept. of Electrical Engineering and Computer Sciences, University of California, Berkeley, CA 94720 USA

[2]Dept. of Electrical Engineering, Stanford University, Stanford, CA 94305 USA

[3]Synopsys, Inc., Mountain View, CA 94043 USA

Tel: +1 (510) 643-2639, Email: heikam@eecs.berkeley.edu

Abstract

An accumulation-mode design for nanometer-scale electromechanical-gate field effect transistors (NEMFETs) is proposed and studied via simulation. In the off state, the gate electrode is in contact with the thin gate dielectric and short-channel effects are effectively suppressed. In the on state, the gate electrode is separated from the thin gate dielectric so that the threshold voltage V_T is dynamically lowered and the transistor drive current I_{on} is enhanced, and gate leakage is eliminated. The NEMFET can likely meet performance specifications for low-power applications at 25 nm gate length, and is attractive for scaled supply voltage operation.

Introduction

A major challenge for CMOS technology scaling is the limited scalability of the MOSFET threshold voltage (V_T) due to the fundamental thermal (k_BT/q) limit that determines the steepest transition (60 mV/dec at 300K) between on and off states. Alternative transistor designs based on band-to-band tunneling [1] and avalanche junction breakdown [2] have been proposed to overcome this limit. However, sub-60 mV/dec subthreshold swing (S) has yet to be demonstrated in a tunneling FET (TFET), and an avalanche-amplification (IMOS) device requires a non-zero drain-to-source voltage to sustain the breakdown current, which limits its application. In this paper, we present a new nanoscale-electro-mechanical-gate field effect transistor (NEMFET) design which utilizes the ultra-abrupt movement of a mechanical beam (the gate electrode) to achieve $S < 60$ mV/dec and thus enhance the transistor on/off current ratio.

Device Structure and Operating Principle

Previously reported suspended-gate FETs [3] utilized an enhancement-mode design, which requires a high gate voltage ($>V_T$) for pull-in to occur and suffers from severe short-channel effects due to weak gate-to-channel coupling in the off state. In contrast, the NEMFET in this work utilizes an accumulation-mode design to achieve improved performance characteristics. Figs. 1 and 2 show schematic cross-sections of the NEMFET in the off state and on state, respectively. The gate electrode is assumed to be anchored on either side of the channel (in/out of the plane of the figures), thus forming a clamped-clamped beam (with a characteristic spring constant k) suspended over the channel. To suppress stiction between the gate and the channel upon contact [4], the NEMFET must be vacuum-encapsulated [5].

In the off state (gate voltage $V_g = 0$ V), the gate electrode is pulled down (so that it contacts the thin gate dielectric) due
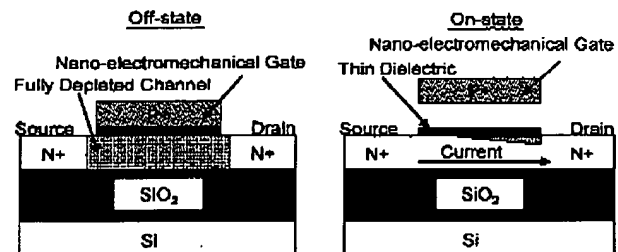

Fig 1. In the off state, the gate is in contact with the thin gate dielectric and the channel is fully depleted, due to the gate-channel work function difference.

Fig 2. In the on state, the gate is separated from the gate dielectric due to the spring restoring force.
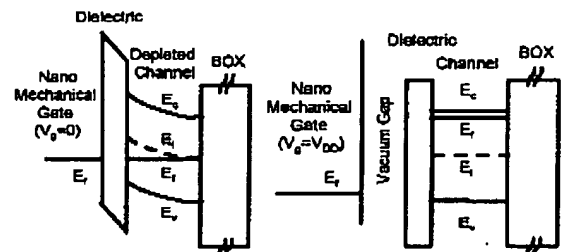

Fig 3. Energy-band diagram for the NEMFET in the off state. Note that the channel is fully depleted.

Fig 4. Energy-band diagram for the NEMFET in the on state. Note that the channel is fully conductive.

to the work-function difference (Φ_{MS}) between the gate and the channel which results in an attractive electrostatic force. The channel region is therefore fully depleted in the off state (Fig. 3). Capacitive coupling between the gate and the channel is therefore maximized to suppress short-channel effects, and the device is in a high-V_T state.

As V_g is increased, the depletion depth in the channel decreases and hence an increasing amount of current can flow between the source and drain regions. V_g also serves to counteract Φ_{MS}, to reduce the attractive electrostatic force between the gate and the channel. At a critical release voltage V_{on} (for which the electrostatic force equals the spring restoring force of the gate), the gate will abruptly pull away from the channel. As a result, the depletion depth decreases and channel current increases abruptly at $V_g = V_{on}$, and the device enters a low-V_T state. Note that the NEMFET mechanically amplifies the modulation of the channel potential by V_g to achieve $S < 60$ mV/dec, in contrast to the TFET and IMOS devices which amplify charge injection. For sufficiently high V_g, the depletion depth is zero; i.e., the

vertical potential drop (V_g - Φ_{MS}) appears entirely across the gap, and the channel film is fully conducting (Fig. 4). A key feature of the NEMFET is that the gate leakage current is zero in the on state, because the gate electrode is physically separated from the channel by a vacuum gap.

NEMFET Modeling

A self-consistent solution for the gap thickness (x) and channel surface potential $\Phi_{s,front}$ can be found by solving the spring-force equation at physical equilibrium and the electrostatic potential equations for the silicon-on-insulator channel layer (Fig. 5) simultaneously and iteratively, for each combination of gate bias V_g and drain bias V_{ds}. (The source is assumed to be grounded.) Note that the average channel potential ($V_{ds}/2$) is considered in the electromechanical model. The data sets (V_g, V_{ds}, x) obtained in this manner were then used, along with the physical device parameters shown in Fig. 6, as input parameters for the ISE device simulator [6] to obtain the potential distribution and drain current for the NEMFET for each data set. This first-order model does not incorporate the van der Waals force between the gate and the channel, since it is highly dependent on the topography of the contacting surfaces [7]. Structuring the contacting surfaces may be necessary to minimize the effect of this additional attractive force.

As shown in Fig. 6, the heavily doped source/drain (S/D) regions are laterally offset from the gate electrode. The offset distance (8.5nm) was chosen to optimize the trade-off between low off-state current and high on-state current. Slight misalignment of the electrode gate to the S/D regions should have negligible impact on transistor performance for the accumulation-mode design.

DC Performance Analysis

Solution of the equations in Fig. 5 yields x as a function of V_g, shown in Fig. 7. It can be seen that x increases abruptly at a critical release voltage (V_{on}) as V_g is increased from 0 V, and that x decreases abruptly at a critical pull-down voltage (V_{off}) as V_g is decreased from a high voltage (1 V). V_{on} and V_{off} are not equal, resulting in hysteresis, because of the quadratic nature of the electrostatic force (ref. Equation (1) in Fig. 5). Qualitatively, the electrostatic force required to hold the gate down is less than that required to pull it down, because of the smaller gap thickness in the pulled-down state. V_{ds} reduces the average applied bias between the gate and the channel, resulting in a stronger attractive electrostatic force; thus V_{on} and V_{off} each increase with V_{ds}. Note that for the range of V_g and V_{ds} values considered here, x is less than or equal to 1 nm, which is the gap thickness as fabricated (t_{gap}).

As shown in Fig. 8, the abrupt movement of the gate results in a correspondingly abrupt change in the channel potential profile at $V_g = V_{on}$. This can be equivalently described as a dynamic reduction in V_T as V_g increases to be higher than V_{on}. If V_T for an accumulation-mode MOSFET is defined as the value of V_g for which the channel is just fully depleted, then the change in V_T due to the movement of the

gate is approximately $\Delta V_T = -qN_B T_{Si} x / \varepsilon_o = 0.36V$, where N_B is the channel/body doping concentration, T_{Si} is the channel film thickness, and ε_o is the vacuum permittivity.

Figs. 9 and 10 show the simulated NEMFET I_d-V_g and I_d-V_d characteristics, respectively. As compared to a fixed-gate accumulation-mode FET with the same on-state current I_{on}, the NEMFET provides more than $10^5\times$ reduction in I_{off}. As compared to a fixed-gate accumulation-mode FET with the

Mechanics: $F_{net} - \varepsilon_o V_{gap}^2 A / (2x^2) \cdot k(t_{gap} - x) = 0$ - (1)

$V_{gap} = V_{FG} - \Phi_{MS,front} - V_{ox} - \Phi_{s,front}$, where $V_{gap}=$ voltage drop across the vacuum gap, k = spring constant of the mechanical gate, $t_{gap}=$ fabricated gap thickness, $V_{ox}=$ voltage drop across the front gate oxide

Electrostatics: $V_{FG} = V_g = \Phi_{MS,front} + (1 + C_{si}/C_{ox,front})\Phi_{s,front}$

$- (C_{si}/C_{ox,front})(\Phi_{s,back} - V_{ds}/2) - Q_{s,front}/C_{ox,front}$

$V_{BG} = 0 = \Phi_{MS,back} + (1 + C_{si}/C_{ox,back})(\Phi_{s,back} - V_{ds}/2)$

$- (C_{si}/C_{ox,back})\Phi_{s,front} - Q_{s,back}/C_{ox,back}$

$$Q_{s,front} = \sqrt{\begin{array}{l} 2\varepsilon_{si}k_BT(\frac{n_i^2}{n_o}(e^{q\Phi_{s,front}/(k_BT)} + q\Phi_{s,front}/(k_BT) - 1) \\ + n_o(e^{q\Phi_{s,front}/(k_BT)} - q\Phi_{s,front}/(k_BT) - 1))) \end{array}}$$

$$Q_{s,back} = \sqrt{\begin{array}{l} 2\varepsilon_{si}k_BT \times \\ (\frac{n_i^2}{n_o}(e^{q(\Phi_{s,back}-V_{ds}/2)/(k_BT)} + q(\Phi_{s,back} - V_{ds}/2)/(k_BT)-1) \\ + n_o(e^{q(\Phi_{s,back}-V_{ds}/2)/(k_BT)} - q(\Phi_{s,back} - V_{ds}/2)/(k_BT) - 1)) \end{array}}$$

$C_{ox,front} = \dfrac{\varepsilon_o}{(t_{ox}/(\varepsilon_{SiO_2}/\varepsilon_o) + x)}$ $C_{ox,back} = \dfrac{\varepsilon_{SiO_2}}{T_{BOX}}$, $C_{si} = \dfrac{\varepsilon_{Si}}{T_{si}}$.

Fig 5. Equilibrium equations for NEMFET mechanics and electrostatics, which are solved simultaneously to obtain the equilibrium gap x.
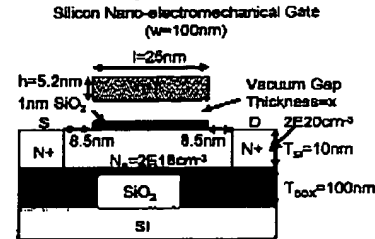
Silicon Nano-electromechanical Gate
(w=100nm)

Fig 6. Cross-section of transistor structure used in device simulations. Default values for channel doping (N_o) and thickness (T_S) are indicated.
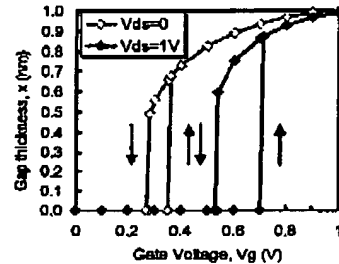
Fig 7. Dependence of gap thickness x on gate and drain voltages. For $V_{ds}=$ 0V, $V_{on} = 0.27V$ and $V_{off} = 0.35V$. V_{on} and V_{off} shift to 0.53V and 0.7V, respectively, for $V_{ds} = 1V$. V_{on} and V_{off} also depend on gate dimensions.

same off-state current I_{off}, the NEMFET provides 30% improvement in on-state current I_{on}. Due to the dependence of V_{on} and V_{off} on V_{ds}, negative differential resistance (NDR), with hysteresis is seen in the I_d-V_d characteristics, for moderate values of V_g. This NDR behavior can potentially be exploited for compact circuit design [8].
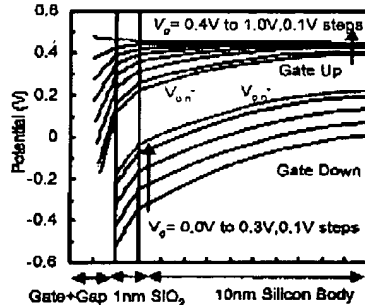
Fig. 8. Potential distribution through the gate dielectric and channel, for increasing values of V_g (V_{ds}= 0V). When the gate is released at V_g – V_{on}, the channel potential profile changes abruptly.
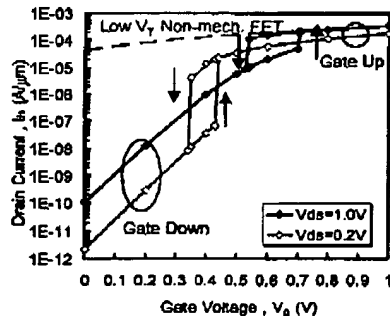
Fig. 9. Simulated NEMFET transfer characteristics. Abrupt changes in current are seen at V_{on} and V_{off} (ref. Fig. 7). I_{on} and I_{off} are 336µA/µm and 110pA/µm, respectively, for V_{ds} = 1V.
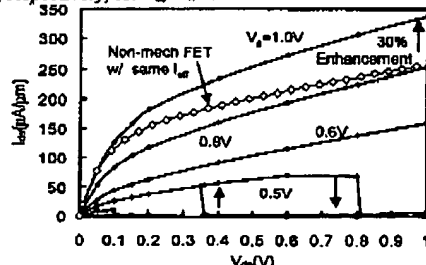
Fig. 10. Simulated NEMFET output characteristics.

Design Optimization

V_{on} and V_{off} must each lie within the subthreshold operation range of V_g in order for the NEMFET to be a dynamic-V_T device. Figs. 11 and 12 show the dependences of V_{on} and V_{off} on N_B and t_{gap}, respectively. The optimal value of N_B lies in the low-10^{18} cm^{-3} range. Note that t_{gap} cannot be much greater than 1 nm; otherwise the gate will not be pulled-down in the off state (at V_g = 0 V). V_{on} and V_{off} will also vary linearly with the gate work function, as does V_T.

Fig. 13 shows how I_{on} and I_{off} change with N_B, for two different values of T_{Si}. N_B must be tightly controlled to minimize performance variation, as is generally the case for accumulation-mode FET designs. Thinner T_{Si} can yield better I_{on}/I_{off}, but at higher N_B which increases V_{on} and V_{off}. With modest enhancement in I_{on} achieved by process-induced strain, the NEMFET can be expected to meet industry performance targets for 25 nm gate length [9].
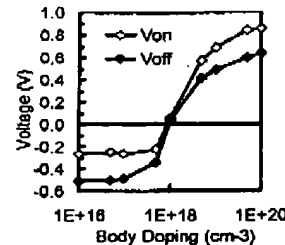
Fig. 11. Dependence of V_{on} and V_{off} on channel/body doping. An increase in N_B increases the work function difference Φ_{MS} and thus a larger gate voltage is needed to release/pull-down the gate electrode.
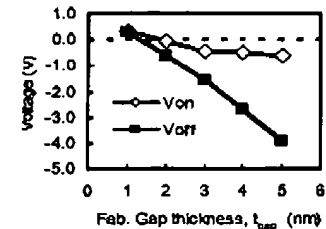
Fig. 12. Dependence of V_{on} and V_{off} on the fabricated gap thickness t_{gap}. A larger initial gap means a larger spring restoring force. Thus, the gate electrode is released/pulled-down at a lower gate voltage.
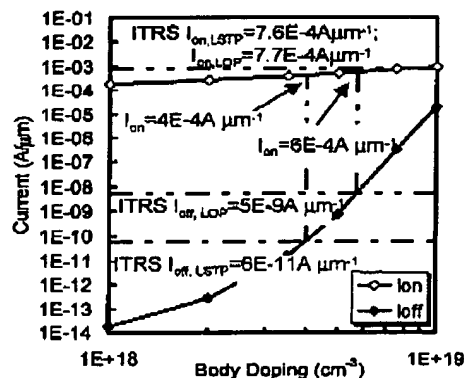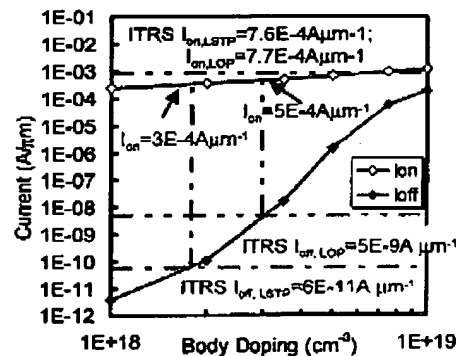
Fig. 13. I_{on} and I_{off} vs. channel/body doping for T_{si} = 10nm (top) and T_{Si} = 8nm (bottom). ITRS targets for low operating power (LOP) and low standby power (LSTP) applications are indicated [9].

AC Performance Analysis

As the effective gate oxide thickness (EOT) changes with the gate voltage, the average gate capacitance of the NEMFET is found by integration:

$$\int_0^{V_{dd}} C_g(V_g)dV_g/V_g \bigg|_{V_{ds}=1V} = 0.66fF/\mu m$$

The spring constant of the gate (k), which is a doubly clamped beam, can be estimated as:

$$k = \frac{16Elh^3}{w^3} = 9.5\mu N/\mu m$$

where E=170GPa is the Young's Modulus of silicon

The dynamic power dissipation of the NEMFET consists of two main parts: the electrical charging/discharging of capacitances ($P_{Electrical}$) and the mechanical deformation of the gate ($P_{Mechanical}$):

$$P_{Electrical} = C_g W V_{DD}^2 f_{0 \to 1}; \quad P_{Mechanical} = \frac{1}{2} k x^2 f_{0 \to 1}$$

Assuming $f_{0 \to 1}=1GHz$: $P_{Electrical} = 66$ nW and $P_{Mechanical} = 4.75$ nW. The mechanical deformation power is thus expected to be a small portion of the total dynamic power dissipation (in the above case ≈ 6.8%), due to the tiny displacement (1 nm) of the mechanical gate.

The switching speed of the NEMFET can be limited by two factors: the speed of the gate movement (inverse resonant frequency $(\sqrt{k/m})^{-1}$, where m is the mass of the mechanical gate) and the intrinsic delay ($C_g V_{DD}/I_{on}$). Under constant ratio scaling, the mass decreases more rapidly than the spring constant of the mechanical gate. So, in the nanoscale regime, the gate resonant frequency can be in the GHz range. For example, the resonant frequency of the gate is 18 GHz for the design (Fig. 6) studied in this work. The intrinsic delay is ~2 ps, however, so that the switching speed of the NEMFET is dictated by the mechanical delay. This will limit its application to <10 GHz operating frequencies.

NEMFET with Scaled Supply Voltage

To leverage fully the benefit of a sub-$k_B T/q$ transistor for low-power electronics, the supply voltage (V_{DD}) should be aggressively scaled down in order to lower dynamic power consumption. Figs. 14 and 15 show the simulated I_d-V_g and I_d-V_d characteristics, respectively, for a NEMFET utilizing a 5.3-nm-thick gate electrode with 5.05 eV work function (e.g. heavily p-type doped silicon-germanium alloy [10]) which provides for lower V_{on} and V_{off}. For a supply voltage of 0.5 V, I_{on} and I_{off} are 104 $\mu A/\mu m$ and 124 pA/μm, respectively. As compared to fixed-gate accumulation-mode FET designs, these represent a 13× improvement in I_{on} or 10^5 reduction in I_{off}.

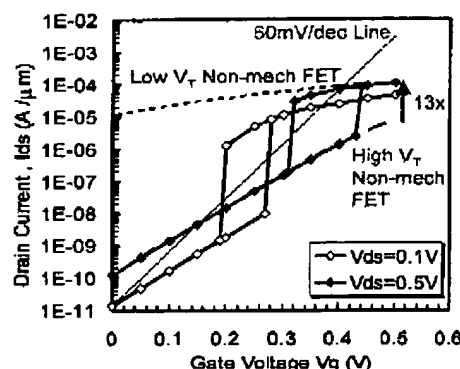
Fig. 14. Simulated NEMFET transfer characteristics for $V_{DD} = 0.5V$. For reference, a line with 60mV/dec slope is shown. Also, the curves for a fixed-gate, high-V_T FET (with same I_{off} as for the NEMFET) and for a fixed-gate, low-V_T FET (with same I_{on} as for the NEMFET) are shown for reference.
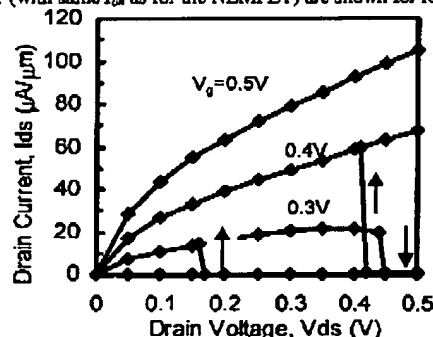

Fig. 15. Simulated NEMFET I_d-V_d output characteristics.

Conclusion

A new accumulation-mode NEMFET device is proposed and is shown to be capable of sub-60 mV/dec switching. Its dynamic-V_T characteristic is advantageous for improving I_{on}/I_{off} and facilitating V_{DD} scaling, and its gate leakage current is zero in the on state. These features make the NEMFET an attractive candidate for low-power electronics applications.

References

[1] T. Nirschl et al., IEDM Tech. Dig., 195 (2004).
[2] K. Gopalakrishnan et al., IEDM Tech. Dig., 289 (2002).
[3] A. M. Ionescu et al., ISQED, 496 (2002)
[4] R. Maboudian et al., J. Vac. Sci. Tech. B 15, 1 (1997).
[5] T. W. Kenny et al., Transducers '05, 1965 (2005).
[6] DESSIS 10.0.6 User's Manual, Synopsys, Inc.
[7] F. Delrio et al, Nature Materials 4, 629 (2005)
[8] P. Mazumder et al., Proc. IEEE 86, 664 (1998).
[9] International Technology Roadmap for Semiconductors, 2004 update (http://public.itrs.net)
[10] T.-J. King et al., IEDM Tech. Dig., 253 (1990).